Analysis of the use of [68Ga]Ga-FAPI and [18F]FDG PET/CT for diagnosing and staging non-small cell lung cancer

Junhao Wu
Southwest Medical University
Hao Deng
Southwest Medical University
Haoshu Zhong
Southwest Medical University
Tao Wang
Southwest Medical University
Kai Zheng
Southwest Medical University
Zijuan Rao
Southwest Medical University
Weidong Gong
Southwest Medical University
Yingwei Wang
Southwest Medical University
Yue Chen
Southwest Medical University
chunyin zhang (zhangchunyin345@sina.com)
Southwest Medical University https://orcid.org/0000-0003-3003-0094

Research Article

Keywords: [68Ga]Ga-FAPI, [18F]FDG, non-small-cell lung cancer (NSCLC), Fibroblast activation protein (FAP)

Posted Date: March 22nd, 2022

DOI: https://doi.org/10.21203/rs.3.rs-1443787/v1

Abstract

Purpose

The current research was developed for comparing the relative diagnostic utility of [^{68}Ga]Ga-FAPI PET/CT and [^{18}F]FDG PET/CT when evaluating initial tumors and metastases in non-small cell lung cancer (NSCLC) patients.

Methods

A prospective analysis of 28 individuals with histopathologically confirmed NSCLC that underwent [^{68}Ga]Ga-FAPI and [^{18}F]FDG PET/CT imaging was conducted. The relative performance of these different imaging modalities was compared based upon visual assessment, rates of cancer detection, and metabolic parameters (target-to-background ratio [TBR], maximum standard uptake value [SUVmax]) for both primary tumors and metastases.

Results

In total, this study enrolled 28 cases (13 male, 15 female; median age: 60.5 years, range: 34–78 years. [^{68}Ga]Ga-FAPI PET/CT imaging was found to more effectively discern both metastases and primary tumors as compared to [^{18}F]FDG PET/CT imaging, detecting more primary tumors (28 vs. 27), as well as metastases present within the lymph nodes (53 vs. 49), pleura (8 vs. 7), liver (4 vs. 1), and bone (41 vs. 35). In contrast, [^{68}Ga]Ga-FAPI PET/CT was not capable of detecting as many adrenal metastases as was [^{18}F]FDG PET/CT imaging (0 vs. 2). The SUVmax and TBR values for [^{68}Ga]Ga-FAPI were substantially superior to those for [^{18}F]FDG in lymph node, pleural, and bone metastases. While the SUVmax for these two imaging approaches was comparable for hepatic metastases, [^{68}Ga]Ga-FAPI exhibited a significantly higher TBR in relation to that of [^{18}F]FDG. [^{68}Ga]Ga-FAPI additionally exhibited greater accuracy than that achieved for [^{18}F]FDG PET/CT when used to conduct NSCLC patient N-staging (80% [8/10] vs. 50% [5/10]) and M-staging (92.9% [26/28] vs. 89.3% [25/28]).

Conclusions

These data highlight the value of [^{68}Ga]Ga-FAPI PET/CT imaging as an approach of diagnosing and staging NSCLC, improving the diagnosis of most metastases and facilitating the superior staging of NSCLC patients relative to that achieved by [^{18}F]FDG PET/CT.

Introduction

Cancer is one of the fundamental threats to human health and well-being, with lung cancer in particular remaining among the most common and deadliest tumors, accounting for 2.2 million and 1.76 million new lung cancer diagnoses and deaths globally each year [1]. Lung cancer is a heterogeneous classification of epithelial malignancy with a range of pathological and clinical manifestations. Broadly speaking, lung cancer cases are subdivided into non-small and small cell lung cancer (NSCLC and SCLC, accordingly). Approximately 85% of all lung cancer cases are NSCLC and NSCLC tumors being further subdivided into adenocarcinomas (50%), squamous cell carcinomas (40%), and large cell lung cancer cases [2–4]. For individuals with stage I – IIIA NSCLC, surgical resection is the optimal therapeutic intervention, but just 20–25% of patients are suited to undergo curative surgical resection [2, 3, 5, 6]. The eligibility of newly diagnosed patients for such treatment is generally dependent on the degree of tumor involvement, with ~ 40% of NSCLC patients exhibiting distant metastases at time of initial diagnosis such that accurate tumor staging is essential and can affect both the prognostic evaluation and treatment of patients [5, 7]. [^{18}F]FDG positron emission tomography/computed tomography (PET/CT) imaging has emerged as the most widely used modality for diagnosing and systemically staging NSCLC cases. However, the utility of this

approach can be limited by insufficient soft-tissue contrast and by elevated levels of physiological background activity in specific organs (such as the liver, brain, and gastrointestinal system). It also has the potential to overlook small lesions or those that are located within organs that exhibit high background activity such as the adrenal glands, resulting in poor specificity [1, 8, 9]. Cancer-associated fibroblasts (CAF) are commonly linked to a poor cancer patient prognosis [10–16]. CAFs frequently express elevated levels of the type II transmembrane serine protease fibroblast-activated protein (FAP) [17–19], which plays key roles in migratory, invasive, and angiogenic activity in oncogenic contexts [20–24]. Recently, novel quinoline FAP-specific inhibitor-based PET tracers have been developed that can be used to precisely target fibrotic and tumor-associated stromal tissue [19, 25, 26]. [^{68}Ga]Ga-FAPI PET/CT exhibits a high degree of intratumoral tracer uptake, low normal tissue uptake, and rapid clearance, thus resulting in excellent tumor visibility and a great target to background ratio [26–29]. In multiple recent reports [18, 19, 25, 27, 28, 30–34], [^{68}Ga]Ga-FAPI PET/CT was demonstrated to aid in the visualization of a diversity of tumors in addition to offering clear advantages as compared to [^{18}F]FDG PET/CT when discerning lymph node, pleural, brain, and bone metastases. There exist a limited number of analyses until now, although, comparing the relative [^{18}F]FDG PET/CT and [^{68}Ga]Ga-FAPI with respect to their utility when diagnosing and/or staging NSCLC. Moreover, the clinical utility of ^{68}Ga-FAPI as a radiotracer for utilization in NSCLC patient imaging applications remains to be established as compared to the utility of [^{18}F]FDG. This study was thus developed to examine the relative performance of [^{18}F]FDG PET/CT and [^{68}Ga]Ga-FAPI for NSCLC diagnosis and staging.

Materials And Methods

Patients

The Ethics Committee of Southwest Medical University Hospital approved the present study, which was conducted from July 2020 - October 2021 (Ethics committee approval No.: 2020035), and all patients signed a written informed consent form. The inclusion criteria for this study were as follows: (1) individuals ≥ 18 years of age; (2) individuals newly diagnosed with NSCLC that had not undergone any previous antitumor treatment; (3) individuals that were willing to undergo both [^{68}Ga]Ga-FAPI PET/CT and [^{18}F]FDG imaging; and (4) individuals that presented the letter of informed satisfaction to take part in. Contributors were excluded if they: (1) underwent < 3 months of follow-up; (2) had undergone antitumor treatment prior to PET/CT imaging; or (3) harbored any other non-NSCLC primary tumors.

Radiotracer preparation

[^{18}F]FDG preparation was conducted employing a Siemens Eclipse HD cyclotron and an automated chemical synthesis system. FAPI-04 precursor (98% pure, MedChemExpress LLC, Shanghai, China) was radiolabeled as follows: dissolution of 50 ug of FAPI-04 was performed in 1 mL of NaAc/HAc buffer (pH 4.0-5.0) and combined with 4 mL of [^{68}Ga]Ga-solution (1.7 GBq). This solution was subsequently heated for 10 min at 80°C, succeeded by separation of the resultant product using a SepPak C-18 column. Column elution was performed using 4 mL of saline and 1 mL of 50% ethanol. The prepared [^{18}F]FDG and [^{68}Ga]Ga-FAPI exhibited > 95% radiochemical purity, and were pyrogen-free and sterile.

PET/CT imaging

Contributors were asked to fast, not received intravenous glucose, and avoid strenuous activity or prolonged exercise for a minimum of 6 h before intravenous [^{18}F]FDG (3.7 MBq/kg) infusion, and patients also needed to have normal blood glucose levels. [^{68}Ga]Ga-FAPI injection (1.85–2.59 MBq/kg) did not necessitate any specific fasting or glycemic preparation. A hybrid PET/CT scanner (uMI780, United Imaging Healthcare, Shanghai, China) was used to conduct all PET/CT imaging ~1 h following radiotracer administration. With the contributor's arms raised above their head, an initial spiral CT scan was conducted from the top of the skull to the upper portion of the mid-thigh (current 120 mA; tube voltage 120 kV; matrix 512 × 512 pixels; slice thickness 3.00 mm; window width 300–500 HU; window level 40–60 HU). PET scanning was subsequently conducted using the same bed position utilized for CT scanning, with 1.5 min/position in 3D acquisition mode and 5–6 bed

positions. The resultant outcomes were transferred to a post-processing workstation (v R002, uWS-MI, United Imaging Healthcare, Shanghai, China). PET attenuation correction was performed using CT data, with PET data reconstruction being conducted based upon an ordered subset estimation maximization algorithm (20 subsets, 2 iterations). The overall condition of each case, such as their body temperature, heart rate, blood pressure, and mental status, was assessed by a nuclear medicine physician within 2 h following injection.

Image review

Two nuclear medicine physicians independently conducted visual, qualitative, and semi-quantitative interpretation of all [^{18}F]FDG PET/CT and [^{68}Ga]Ga-FAPI images. Discrepancies were resolved through discussion and consensus. Patient PET/CT images were assessed in the coronal, axial, and sagittal planes. Positive lesions were identified by areas of non-physiological uptake above background in [^{68}Ga]Ga-FAPI PET or [^{18}F]FDG images. Positive lesions were combined with data from the corresponding CT scan images for further diagnosis, and their length were measured and recorded. Positive PET/CT lesions were further categorized as non-malignant lesions, primary tumors, distant metastases, or lymph node metastases. [^{18}F]FDG PET/CT and [^{68}Ga]Ga-FAPI imaging results were initially compared via a visual assessment in which the two images for each patient were assessed to establish their relative inferiority or superiority when detecting primary tumors (based upon tumor size and conspicuousness) and metastatic lesions (based upon numbers, involvement, and conspicuousness). Semi-quantitative analyses were then conducted by comparing [^{18}F]FDG and [^{68}Ga]Ga-FAPI radiotracer uptake within the same lesions. SUVmax was measured using the analytical workstation after the region of interest (ROI) surrounding the lesion had been defined by a physician. The TBR was defined as the difference in radiotracer uptake between the lesion and background, and was measured via dividing the SUVmax for a given lesion by the mean normalized uptake (SUVmean) for normal background tissue.

Diagnostic criteria

Histopathological findings were used for final diagnostic determinations for all primary tumors. When histopathological results were not available for metastases, final diagnosis was made based upon the results derived from multiple imaging modalities (MRI, enhanced CT, ultrasound, bone scan, PET/CT) and corresponding follow-up imaging. During follow-up, a suspicious lesion was considered to be malignant if it exhibited progressive growth or the number and/or size of suspect lesions declined following antitumor treatment.

Statistical Analysis

Statistical evaluations were executed using SPSS (v 26.0; IBM, NY, USA). General data were compared through descriptive analyses, with categorical variables being listed as numbers with percentages, while continuous variables were listed as the mean ± SD. Chi-squared tests were used to compare numbers of positive lesions. Student's t-tests were employed for comparing SUVmax and TBR values for specific lesions associated with [^{68}Ga]Ga-FAPI PET/CT and [^{18}F]FDG imaging. Correlations between lesion length and metabolic parameters (TBR and SUVmax) were assessed through Spearman's rank correlation analyses. A two-tailed $P < 0.05$ was the threshold of significance.

Results

Generally, this study enrolled 28 cases (13 male, 15 female; median age: 60.5 years, range: 34-78 years). The basic features of these cases are detailed in **Table 1**.

The patients had been newly diagnosed with NSCLC, including 24 patients diagnosed with adenocarcinomas and 5 diagnosed with squamous cell carcinomas, with one patient (patient 17) having been simultaneously diagnosed with two primary tumors. In total, 16 patients underwent surgical resection, with 10 having simultaneously undergone mediastinal lymph node dissection. The remaining 12 patients underwent non-surgical antitumor treatment. Genetic testing was

performed for 6 patients, of whom 3 were found to harbor tumors with epidermal growth factor receptor (EGFR) mutations, while 3 harbored wild-type adenocarcinomas.

Table 1 Basic patient characteristics

NO.	Sex	Age	Pathology	Primary tumor site	Metastases site	TMN
1	F	44	ADC	right upper lobe	LNM; LM; PM	T4N2M1a
2	M	61	ADC	left upper lobe	LNM; AM	T1N3M1b
3	M	66	ADC	right upper lobe	None	T1N0M0
4	F	46	ADC	left upper lobe	LNM; BM	T1N3M1c
5	F	48	SCC	left lower lobe	None	T2N0M0
6	F	57	ADC	left lower lobe	LNM; HM; BM	T2N3M1c
7	F	53	ADC	left upper lobe	None	T1N0M0
8	F	72	ADC	right upper lobe	None	T1N0M0
9	M	70	ADC	right upper lobe	None	T1N0M0
10	F	78	ADC	left lower lobe	LM; PM; BM	T4N0M1b
11	M	68	ADC	left upper lobe	LNM	T1N2M0
12	F	57	ADC	right middle lobe	LNM	T1N3M0
13	M	69	SCC	right lower lobe	None	T2N0M0
14	M	49	ADC	right upper/ lower lobe	LNM, Pancreas, Kidney	T4N3M1c
15	F	46	ADC	right middle lobe	LNM	T2N3M0
16	M	63	ADC	left lower lobe	BM	T2N0M1c
17	F	68	ADC ADC	right lower lobe right middle lobe	LNM	T2N2M0
18	M	63	ADC	left upper lobe	LNM;HM; BM	T1N3M1c
19	M	71	SCC	right upper lobe	LNM; BM	T2N3M1b
20	M	67	SCC	right upper lobe	AM	T1N0M1b
21	M	34	ADC	right lower lobe	LNM; BM	T4N3M1c
22	F	58	ADC	right lower lobe	LNM; PM	T2N3M1a
23	F	61	ADC	left upper lobe	LNM	T2N1M0
24	F	60	ADC	right upper lobe	None	T2N0M0
25	M	56	SCC	left lower lobe	LNM	T3N2M0
26	F	45	ADC	right middle lobe	None	T1N0M0
27	F	53	ADC	right upper lobe	None	T1N0M0
28	M	68	ADC	right upper lobe	None	T1N0M0

SCC = squamous cell carcinoma; ADC = adenocarcinoma; LNM = lymph node metastasis; LM = lung metastasis; PM = Pleural metastasis; AM = adrenal metastasis; BM = bone metastasis; HM = hepatic metastases

Adverse event

No patients developed any adverse events, discomfort, or abnormalities with respect to heart rate, body temperature, blood pressure, or mental status within 2 h following imaging agent injection.

Comparison of visual assessment outcomes

Upon visual assessment, [^{68}Ga]Ga-FAPI PET/CT enabled clearer metastatic and primary tumor visualization as compared to [^{18}F]FDG PET/CT in a majority of patients. Specifically, [^{68}Ga]Ga-FAPI outperformed [^{18}F]FDG PET/CT for the visual evaluation of primary tumors (14/28 [50.0%] vs. 9/28 [32.1%]), lymph node metastases (9/15 [60.0%] vs. 5/15 [33.3%]), pleural metastases (3/3 [100.0%] vs. 0/3 [0%]), hepatic metastases (2/2 [100.0%] vs. 0/2 [0%]), and bone metastases (6/7 [85.7%] vs. 0/7 [0%]), but it performed less effectively for pulmonary (0/2 [0%] vs. 2/2 [100.0%]) and adrenal metastases (0/2 [0%] vs. 2/2 [100.0%]) (**Fig 1**).

Patient-based detection rate comparison

The primary tumor detection rates for [^{68}Ga]Ga-FAPI and [^{18}F]FDG PET/CT were similar in patient-based analyses (96.4% [27/28] vs. 92.9% [26/28]), as were the rates of detection for lymph node (93.3% [14/15] vs. 93.3% [14/15]), pulmonary (100% [2/2] vs. 100% [2/2]), pleural (100% [3/3] vs. 100% [3/3]), hepatic (100% [2/2] vs. 50% [1/2]), and bone metastases (100% [7/7] vs. 85.7% [6/7]). [^{68}Ga]Ga-FAPI was discovered to be inferior to [^{18}F]FDG PET/CT when used to detect adrenal metastases, however (0% [0/2] vs. 100% [2/2]) (**Table 2**).

Lesion-based detection rates

[^{68}Ga]Ga-FAPI outperformed [^{18}F]FDG PET/CT in a lesion-based analysis when detecting hepatic (100% [4/4] vs. 25% [1/4]) and bone metastases (97.6% [41/42] vs. 83.3% [35/42]), whereas [^{68}Ga]Ga-FAPI was inferior to [^{18}F]FDG PET/CT when utilized to detect adrenal metastases (0% [0/2] vs. 100% [2/2]). Both approaches performed similarly when used to detect primary tumors (96.6% [28/29] vs. 93.1% [27/29]), as well as lymph node (93.0% [53/57] vs. 86.0% [49/57]), pulmonary (100% [3/3] vs. 100% [3/3]), and pleural metastases (100% [8/8] vs. 87.5% [7/8]) (**Table 2**).

Table 2 Comparison of [^{68}Ga]Ga-FAPI and [^{18}F]FDG PET/CT semi-quantitative imaging parameters

Parameter	Imaging method	primary tumor	Lymph node metastasis	Lung metastasis	Pleural metastasis	Hepatic metastasis	Adrenal metastasis	Bone metastasis
Patient-based analysis		28	15	2	3	2	2	7
No. of patients	^{68}Ga-FAPI	27	14	2	3	2	0	7
	^{18}F-FDG	26	14	2	3	1	2	6
	P	0.553	1.000	1.000	1.000	1.000	0.046	0.299
Lesion-based analysis		29	57	3	8	4	2	42
No. of lesions	^{68}Ga-FAPI	28	53	3	8	4	0	41
	^{18}F-FDG	27	49	3	7	1	2	35
	P	0.554	0.222	1.000	0.302	0.028	0.046	0.026
SUVmax	^{68}Ga-FAPI	9.3 ± 4.6	8.4 ± 4.3	2.4 ± 1.6	10.8 ± 3.6	6.2 ± 2.1	1.2 ± 0.4	11.2 ± 5.5
	^{18}F-FDG	9.9 ± 6.9	6.4 ± 4.7	2.9 ± 1.9	5.5 ± 3.0	3.4 ± 0.27	6.4 ± 3.3	6.5 ± 3.9
	P	0.631	0.003	0.192	0.001	0.062	0.237	0.001
TBR	^{68}Ga-FAPI	26.3 ± 18.8	10.6 ± 6.3	3.4 ± 1.8	9.1 ± 2.8	11.4 ± 5.3	1.6 ± 0.1	16.2 ± 11.2
	^{18}F-FDG	24.0 ± 21.6	6.1 ± 4.9	4.8 ± 3.2	6.2 ± 3.3	1.3 ± 0.3	3.3 ± 2.5	5.9 ± 5.8
	P	0.589	0.001	0.215	0.001	0.027	0.500	0.001

Quantitative analysis of [^{68}Ga]Ga-FAPI and [^{18}F]FDG PET/CT metabolic imaging parameters

The SUVmax and TBR values for [^{18}F]FDG PET/CT and [^{68}Ga]Ga-FAPI did not differ significantly when used for detecting primary tumors, pulmonary metastases, and adrenal metastases, while the SUVmax and TBR of [^{68}Ga]Ga-FAPI were substantially superior to those for [^{18}F]FDG PET/CT when used to discern lymph node, pleural, and bone metastases. When the SUVmax for these two imaging modalities did not differ significantly in the detection of hepatic metastases (P = 0.062), [^{68}Ga]Ga-FAPI was correlated with a remarkably greater TBR value relative to that for [^{18}F]FDG (P = 0.027) (**Table 2**).

The relationship between lesion length and SUVmax values

Significant correlations between lesion length and [^{68}Ga]Ga-FAPI SUVmax values were noted for primary tumors, lymph node metastases, and bone metastases in Spearman's correlation analyses, while [^{18}F]FDG SUVmax values were only correlated with lesion length for primary tumors and lymph node metastases but not for bone metastases (**Fig 2**).

Prediction of *EGFR* mutation status

For six patients with lung adenocarcinoma who underwent genetic testing, the metabolic parameters (SUVmax, TBR) of two imaging modalities were lower in *EGFR* mutant than wild-type lung adenocarcinoma, although neither was significantly different (**Fig 3**).

N and M staging

Overall, 10 NSCLC cases in the current researh cohort underwent mediastinal lymph node dissection (patients 5, 8, 11, 17, 20, 23, 24, 26, 27, and 28). While 19 FDG-positive lymph nodes were found to be benign upon biopsy, just 4 FAPI-positive lymph nodes were confirmed to be benign. For these patients, [^{18}F]FDG PET/CT and [^{68}Ga]Ga-FAPI PET/CT results were consistent with N staging in 8 and 5 patients, respectively. [^{68}Ga]Ga-FAPI PET/CT imaging led to a lower N-stage in 1 patient (patient 11) owing to overlooked lymph node metastases and a higher N-stage in 1 patient (patient 28) owing to the detection of additional false-positive lymph nodes. In contrast, [^{18}F]FDG PET/CT detected additional false-positive lymph nodes in 5 patients (patients 11, 20, 23, 27, and 28) resulting in higher N staging for these individuals. Overall, NSCLC patient N-staging based upon [^{68}Ga]Ga-FAPI results was more accurate than [^{18}F]FDG PET/CT results for these same patients (80% [8/10] vs. 50% [5/10]).

Of the contributors considered in the present research, 12 (42.9%) exhibited distant metastatic lesions, while 16 (57.1%) did not. [^{68}Ga]Ga-FAPI PET/CT enabled the accurate M-staging of 26 of these patients, while its failure to detect adrenal metastases results in a decreased M stage in 2 individuals (patients 2 and 20). [^{18}F]FDG PET/CT enabled the accurate M-staging of 25 patients, with incorrect results in the remaining patients owing to 1 instance of false-positive adrenal modules (patient 13) and 2 instances of false-negative bone metastases (patients 16 and 21). The overall M-staging accuracy of [^{68}Ga]Ga-FAPI PET/CT was superior to that of [^{18}F]FDG PET/CT (92.9% [26/28] vs. 89.3% [25/28]).

Discussion

The current exploration was conducted for exploring the comparative ability of [^{68}Ga]Ga-FAPI and [^{18}F]FDG PET/CT to diagnose and stage NSCLC patients. Overall, these results suggest that [^{68}Ga]Ga-FAPI can more clearly image primary tumors and metastatic lesions as compared to [^{18}F]FDG PET/CT (**Fig 4**). [^{68}Ga]Ga-FAPI exhibited excellent detection rates for primary tumors and most metastatic lesions, particularly for hepatic and bone metastases (**Fig 5**). Importantly, owing to the higher levels of [^{68}Ga]Ga-FAPI tracer uptake in both primary tumors and the majority of metastatic lesions, this imaging modality is better equipped to detect smaller lesions at an earlier stage in their development. Reduced physiological uptake of this tracer also reduces the odds of overlooking hepatic or bone metastases. According to semi-quantitative assessments, [^{68}Ga]Ga-FAPI PET/CT SUVmax and TBR values were substantially superior to those for [^{18}F]FDG PET/CT when analyzing metastases present in the lymph nodes, pleura, and bone. While the SUVmax values for these two imaging modalities did not differ significantly when evaluating hepatic metastases, the TBR value for FAPI was significantly superior to that for FDG owing to lower levels of background FAPI uptake in the liver.

One recent analysis [31] comparing [^{68}Ga]Ga-FAPI and [^{18}F]FDG reported no significant differences between these two technologies with respect to primary lung cancer detection rates or associated SUVmax or TBR values, in line with our findings. In contrast, Wang et al. [35] reported that [^{68}Ga]Ga-FAPI yielded significantly higher SUVmax and TBR values as compared to [^{18}F]FDG PET/CT, leading them to conclude that this former technology is better suited to the detection of early-stage lung cancer. AS their analysis specifically included individuals with large tumors (Mean size: 3.3 cm) and advanced disease, this may account for their inconsistent results. Further large-scale clinical research is still necessary to thoroughly verify the utility of [^{68}Ga]Ga-FAPI PET/CT as a tool for evaluating primary NSCLC tumors. We additionally explored the potential relevance of key metabolic parameters as predictors of primary tumor *EGFR* mutation status, and found that both the SUVmax and TBR values were lower in *EGFR*-mutant lung adenocarcinoma relative to wild-type lung adenocarcinoma for both tested imaging modalities, although these differences were not significant. Zhu et al.

[36] previously demonstrated that [^{18}F]FDG PET/CT-derived quantitative criteria offer moderate efficacy when used to predict lung adenocarcinoma *EGFR* mutation status, in line with our results. Our data further suggest that the metabolic parameters derived from [^{68}Ga]Ga-FAPI imaging may also be effective predictors of *EGFR* mutations. However, given the limited number of patients that underwent genetic testing in the current exploration, the predictive relevance of these [^{68}Ga]Ga-FAPI PET/CT-derived parameters in the context of *EGFR* mutation status warrant further investigation.

At present, surgical tumor resection is the benchmark of care for early-stage NSCLC patients. The capability of predicting and detecting regional lymph node metastases in these patients performs a central task in treatment planning and associated management efforts [37]. While [^{18}F]FDG PET/CT imaging is frequently employed as a screening tool to stage lung cancer patients, it exhibits relatively low sensitivity for small metastatic lesions located within lymph nodes [8, 9]. In contrast, it was discovered that [^{68}Ga]Ga-FAPI PET/CT was capable of detecting lymph node metastases more reliably than was [^{18}F]FDG PET/CT, yielding higher SUVmax and TBR values for these metastases relative to the latter imaging modality (**Fig 6**). This achievement is in agreement with data published previously through Wang et al [35]. As [^{68}Ga]Ga-FAPI PET/CT imaging can detect lymph node metastases at an earlier stage, it has the potential to increase occult lymph node metastasis detection, guiding the more accurate staging of NSCLC patients. Mediastinal false-positive lymph node detection rates were also lower for [^{68}Ga]Ga-FAPI relative to [^{18}F]FDG PET/CT, consistent with the higher specificity of the former technique (**Fig 7**), potentially reducing rates of unnecessary treatment in individuals with NSCLC.

Our analyses additionally revealed [^{68}Ga]Ga-FAPI imaging to be superior to [^{18}F]FDG PET/CT when used for the detection of hepatic, pleural, and bone metastases, in line with prior evidence [28, 35, 38, 39]. This is ascribable to the reduced physiological uptake of the ^{68}Ga-FAPI radiotracer and associated sensitivity gains. High levels of hepatic glucose metabolism have the potential to mask FDG uptake by metastatic lesions within this organ, while the use of [^{68}Ga]Ga-FAPI PET/CT may enable the more reliable detection of these lesions. [^{68}Ga]Ga-FAPI PET/CT is also capable of facilitating the early detection of occult bone and pleural metastases to guide more appropriate patient staging and treatment efforts (**Fig 8**). We further discovered that [^{68}Ga]Ga-FAPI PET/CT exhibited low sensitivity when used to detect adrenal metastases, suggesting that such lesions may be not associated with substantial fibrotic activity. However, [^{18}F]FDG PET/CT imaging also exhibited poor sensitivity for these metastases, suggesting that diagnosing adrenal metastases necessitates a combination of CT imaging and other interrogative modalities to ensure accuracy.

There are multiple limitations to the present analysis. For one, the number of included contributors was relatively small, and the variety of NSCLC pathological types was limited, thus potentially contributing to some degree of bias in the overall study results. Second, accurate pathological results were not available for many suspicious metastatic lesions in individuals with advanced NSCLC as it is generally impractical and unethical to conduct biopsies of these samples. Third, the minimum follow-up duration for patients in this study was just 3 months, and future studies should thus utilize an extended follow-up interval.

Conclusion

In summary, these results indicate that [^{68}Ga]Ga-FAPI PET/CT imaging demonstrates desirable performances when used to detect both primary tumors and most metastatic lesion types in individuals diagnosed with NSCLC. Moreover, [^{68}Ga]Ga-FAPI exhibits significantly better diagnostic efficacy relative to that of [^{18}F]FDG PET/CT imaging when used to detect metastatic lesions in the lymph nodes, pleura, liver, and bone. [^{68}Ga]Ga-FAPI PET/CT, therefore, holds promise as a viable clinical approach to NSCLC patient diagnosis, staging, and treatment planning that is likely to replace [^{18}F]FDG PET/CT in the future.

Declarations

Compliance with ethical standards

Conflict of interest All authors declare that they have no conflict of interest.

Ethics approval All procedures involving human participants were performed in accordance with the ethical standards ofthe institutional and/or national research committee, as well as the 1964 Helsinki Declaration and its later amendments or comparable ethical standards. This article does not contain any animal experiments.

Consent to participate Informed consent was obtained from all participants included in the study.

Consent for publication Informed consent was obtained from all participants included in the study.

Code availability Not applicable.

References

1. Thai AA, Solomon BJ, Sequist LV, Gainor JF, Heist RS. Lung cancer. Lancet. 2021;398(10299):535-54. doi:10.1016/S0140-6736(21)00312-3.
2. Group NM-aC, Arriagada R, Auperin A, Burdett S, Higgins JP, Johnson DH et al. Adjuvant chemotherapy, with or without postoperative radiotherapy, in operable non-small-cell lung cancer: two meta-analyses of individual patient data. Lancet. 2010;375(9722):1267-77. doi:10.1016/S0140-6736(10)60059-1.
3. Zhong WZ, Wang Q, Mao WM, Xu ST, Wu L, Shen Y et al. Gefitinib versus vinorelbine plus cisplatin as adjuvant treatment for stage II-IIIA (N1-N2) EGFR-mutant NSCLC (ADJUVANT/CTONG1104): a randomised, open-label, phase 3 study. Lancet Oncol. 2018;19(1):139-48. doi:10.1016/S1470-2045(17)30729-5.
4. Han Y, Ma Y, Wu Z, Zhang F, Zheng D, Liu X et al. Histologic subtype classification of non-small cell lung cancer using PET/CT images. Eur J Nucl Med Mol Imaging. 2021;48(2):350-60. doi:10.1007/s00259-020-04771-5.
5. Dwamena BA, Sonnad SS, Angobaldo JO, Wahl RL. Metastases from non-small cell lung cancer: mediastinal staging in the 1990s--meta-analytic comparison of PET and CT. Radiology. 1999;213(2):530-6. doi:10.1148/radiology.213.2.r99nv46530.
6. Le Pechoux C, Pourel N, Barlesi F, Lerouge D, Antoni D, Lamezec B et al. Postoperative radiotherapy versus no postoperative radiotherapy in patients with completely resected non-small-cell lung cancer and proven mediastinal N2 involvement (Lung ART): an open-label, randomised, phase 3 trial. Lancet Oncol. 2022;23(1):104-14. doi:10.1016/S1470-2045(21)00606-9.
7. Machado Medeiros T, Altmayer S, Watte G, Zanon M, Basso Dias A, Henz Concatto N et al. 18F-FDG PET/CT and whole-body MRI diagnostic performance in M staging for non-small cell lung cancer: a systematic review and meta-analysis. Eur Radiol. 2020;30(7):3641-9. doi:10.1007/s00330-020-06703-1.
8. Reck M, Heigener DF, Mok T, Soria JC, Rabe KF. Management of non-small-cell lung cancer: recent developments. Lancet. 2013;382(9893):709-19. doi:10.1016/S0140-6736(13)61502-0.
9. Huellner MW, de Galiza Barbosa F, Husmann L, Pietsch CM, Mader CE, Burger IA et al. TNM Staging of Non-Small Cell Lung Cancer: Comparison of PET/MR and PET/CT. J Nucl Med. 2016;57(1):21-6. doi:10.2967/jnumed.115.162040.
10. Chen L, Chen M, Han Z, Jiang F, Xu C, Qin Y et al. Clinical significance of FAP-alpha on microvessel and lymphatic vessel density in lung squamous cell carcinoma. J Clin Pathol. 2018;71(8):721-8. doi:10.1136/jclinpath-2017-204872.
11. Sandberg TP, Stuart M, Oosting J, Tollenaar R, Sier CFM, Mesker WE. Increased expression of cancer-associated fibroblast markers at the invasive front and its association with tumor-stroma ratio in colorectal cancer. BMC Cancer. 2019;19(1):284. doi:10.1186/s12885-019-5462-2.
12. Wong PF, Wei W, Gupta S, Smithy JW, Zelterman D, Kluger HM et al. Multiplex quantitative analysis of cancer-associated fibroblasts and immunotherapy outcome in metastatic melanoma. J Immunother Cancer. 2019;7(1):194.

doi:10.1186/s40425-019-0675-0.

13. Kim MG, Shon Y, Kim J, Oh YK. Selective Activation of Anticancer Chemotherapy by Cancer-Associated Fibroblasts in the Tumor Microenvironment. J Natl Cancer Inst. 2017;109(1). doi:10.1093/jnci/djw186.
14. Sukowati CH, Anfuso B, Croce LS, Tiribelli C. The role of multipotent cancer associated fibroblasts in hepatocarcinogenesis. BMC Cancer. 2015;15:188. doi:10.1186/s12885-015-1196-y.
15. Kieffer Y, Hocine HR, Gentric G, Pelon F, Bernard C, Bourachot B et al. Single-Cell Analysis Reveals Fibroblast Clusters Linked to Immunotherapy Resistance in Cancer. Cancer Discov. 2020;10(9):1330-51. doi:10.1158/2159-8290.CD-19-1384.
16. Paulsson J, Micke P. Prognostic relevance of cancer-associated fibroblasts in human cancer. Semin Cancer Biol. 2014;25:61-8. doi:10.1016/j.semcancer.2014.02.006.
17. Shangguan C, Gan G, Zhang J, Wu J, Miao Y, Zhang M et al. Cancer-associated fibroblasts enhance tumor (18)F-FDG uptake and contribute to the intratumor heterogeneity of PET-CT. Theranostics. 2018;8(5):1376-88. doi:10.7150/thno.22717.
18. Chen H, Zhao L, Ruan D, Pang Y, Hao B, Dai Y et al. Usefulness of [(68)Ga]Ga-DOTA-FAPI-04 PET/CT in patients presenting with inconclusive [(18)F]FDG PET/CT findings. Eur J Nucl Med Mol Imaging. 2021;48(1):73-86. doi:10.1007/s00259-020-04940-6.
19. Loktev A, Lindner T, Mier W, Debus J, Altmann A, Jager D et al. A Tumor-Imaging Method Targeting Cancer-Associated Fibroblasts. J Nucl Med. 2018;59(9):1423-9. doi:10.2967/jnumed.118.210435.
20. Chen WT, Kelly T. Seprase complexes in cellular invasiveness. Cancer Metastasis Rev. 2003;22(2-3):259-69. doi:10.1023/a:1023055600919.
21. Huang Y, Wang S, Kelly T. Seprase promotes rapid tumor growth and increased microvessel density in a mouse model of human breast cancer. Cancer Res. 2004;64(8):2712-6. doi:10.1158/0008-5472.can-03-3184.
22. Yang X, Lin Y, Shi Y, Li B, Liu W, Yin W et al. FAP Promotes Immunosuppression by Cancer-Associated Fibroblasts in the Tumor Microenvironment via STAT3-CCL2 Signaling. Cancer Res. 2016;76(14):4124-35. doi:10.1158/0008-5472.CAN-15-2973.
23. Nawrocka D, Krzyscik MA, Opalinski L, Zakrzewska M, Otlewski J. Stable Fibroblast Growth Factor 2 Dimers with High Pro-Survival and Mitogenic Potential. Int J Mol Sci. 2020;21(11). doi:10.3390/ijms21114108.
24. Bainbridge TW, Dunshee DR, Kljavin NM, Skelton NJ, Sonoda J, Ernst JA. Selective Homogeneous Assay for Circulating Endopeptidase Fibroblast Activation Protein (FAP). Sci Rep. 2017;7(1):12524. doi:10.1038/s41598-017-12900-8.
25. Kratochwil C, Flechsig P, Lindner T, Abderrahim L, Altmann A, Mier W et al. (68)Ga-FAPI PET/CT: Tracer Uptake in 28 Different Kinds of Cancer. J Nucl Med. 2019;60(6):801-5. doi:10.2967/jnumed.119.227967.
26. Giesel FL, Kratochwil C, Lindner T, Marschalek MM, Loktev A, Lehnert W et al. (68)Ga-FAPI PET/CT: Biodistribution and Preliminary Dosimetry Estimate of 2 DOTA-Containing FAP-Targeting Agents in Patients with Various Cancers. J Nucl Med. 2019;60(3):386-92. doi:10.2967/jnumed.118.215913.
27. Pang Y, Zhao L, Luo Z, Hao B, Wu H, Lin Q et al. Comparison of (68)Ga-FAPI and (18)F-FDG Uptake in Gastric, Duodenal, and Colorectal Cancers. Radiology. 2021;298(2):393-402. doi:10.1148/radiol.2020203275.
28. Chen H, Pang Y, Wu J, Zhao L, Hao B, Wu J et al. Comparison of [(68)Ga]Ga-DOTA-FAPI-04 and [(18)F] FDG PET/CT for the diagnosis of primary and metastatic lesions in patients with various types of cancer. Eur J Nucl Med Mol Imaging. 2020;47(8):1820-32. doi:10.1007/s00259-020-04769-z.
29. Koerber SA, Staudinger F, Kratochwil C, Adeberg S, Haefner MF, Ungerechts G et al. The Role of (68)Ga-FAPI PET/CT for Patients with Malignancies of the Lower Gastrointestinal Tract: First Clinical Experience. J Nucl Med. 2020;61(9):1331-6. doi:10.2967/jnumed.119.237016.
30. Wei Y, Cheng K, Fu Z, Zheng J, Mu Z, Zhao C et al. [(18)F]AlF-NOTA-FAPI-04 PET/CT uptake in metastatic lesions on PET/CT imaging might distinguish different pathological types of lung cancer. Eur J Nucl Med Mol Imaging. 2021.

doi:10.1007/s00259-021-05638-z.

31. Lan L, Liu H, Wang Y, Deng J, Peng D, Feng Y et al. The potential utility of [(68) Ga]Ga-DOTA-FAPI-04 as a novel broad-spectrum oncological and non-oncological imaging agent-comparison with [(18)F]FDG. Eur J Nucl Med Mol Imaging. 2022;49(3):963-79. doi:10.1007/s00259-021-05522-w.
32. Gu B, Xu X, Zhang J, Ou X, Xia Z, Guan Q et al. The Added Value of (68)Ga-FAPI-04 PET/CT in Patients with Head and Neck Cancer of Unknown Primary with (18)F-FDG Negative Findings. J Nucl Med. 2021. doi:10.2967/jnumed.121.262790.
33. Syed M, Flechsig P, Liermann J, Windisch P, Staudinger F, Akbaba S et al. Fibroblast activation protein inhibitor (FAPI) PET for diagnostics and advanced targeted radiotherapy in head and neck cancers. Eur J Nucl Med Mol Imaging. 2020;47(12):2836-45. doi:10.1007/s00259-020-04859-y.
34. Zhao L, Chen S, Lin L, Sun L, Wu H, Lin Q et al. [(68)Ga]Ga-DOTA-FAPI-04 improves tumor staging and monitors early response to chemoradiotherapy in a patient with esophageal cancer. Eur J Nucl Med Mol Imaging. 2020;47(13):3188-9. doi:10.1007/s00259-020-04818-7.
35. Wang L, Tang G, Hu K, Liu X, Zhou W, Li H et al. Comparison of (68)Ga-FAPI and (18)F-FDG PET/CT in the Evaluation of Advanced Lung Cancer. Radiology. 2022:211424. doi:10.1148/radiol.211424.
36. Zhu L, Yin G, Chen W, Li X, Yu X, Zhu X et al. Correlation between EGFR mutation status and F(18) -fluorodeoxyglucose positron emission tomography-computed tomography image features in lung adenocarcinoma. Thorac Cancer. 2019;10(4):659-64. doi:10.1111/1759-7714.12981.
37. Li ZM, Ding ZP, Luo QQ, Wu CX, Liao ML, Zhen Y et al. Prognostic significance of the extent of lymph node involvement in stage II-N1 non-small cell lung cancer. Chest. 2013;144(4):1253-60. doi:10.1378/chest.13-0073.
38. Zhao L, Pang Y, Zheng H, Han C, Gu J, Sun L et al. Clinical utility of [(68)Ga]Ga-labeled fibroblast activation protein inhibitor (FAPI) positron emission tomography/computed tomography for primary staging and recurrence detection in nasopharyngeal carcinoma. Eur J Nucl Med Mol Imaging. 2021;48(11):3606-17. doi:10.1007/s00259-021-05336-w.
39. Wu J, Wang Y, Liao T, Rao Z, Gong W, Ou L et al. Comparison of the Relative Diagnostic Performance of [(68)Ga]Ga-DOTA-FAPI-04 and [(18)F]FDG PET/CT for the Detection of Bone Metastasis in Patients With Different Cancers. Front Oncol. 2021;11:737827. doi:10.3389/fonc.2021.737827.

Figures

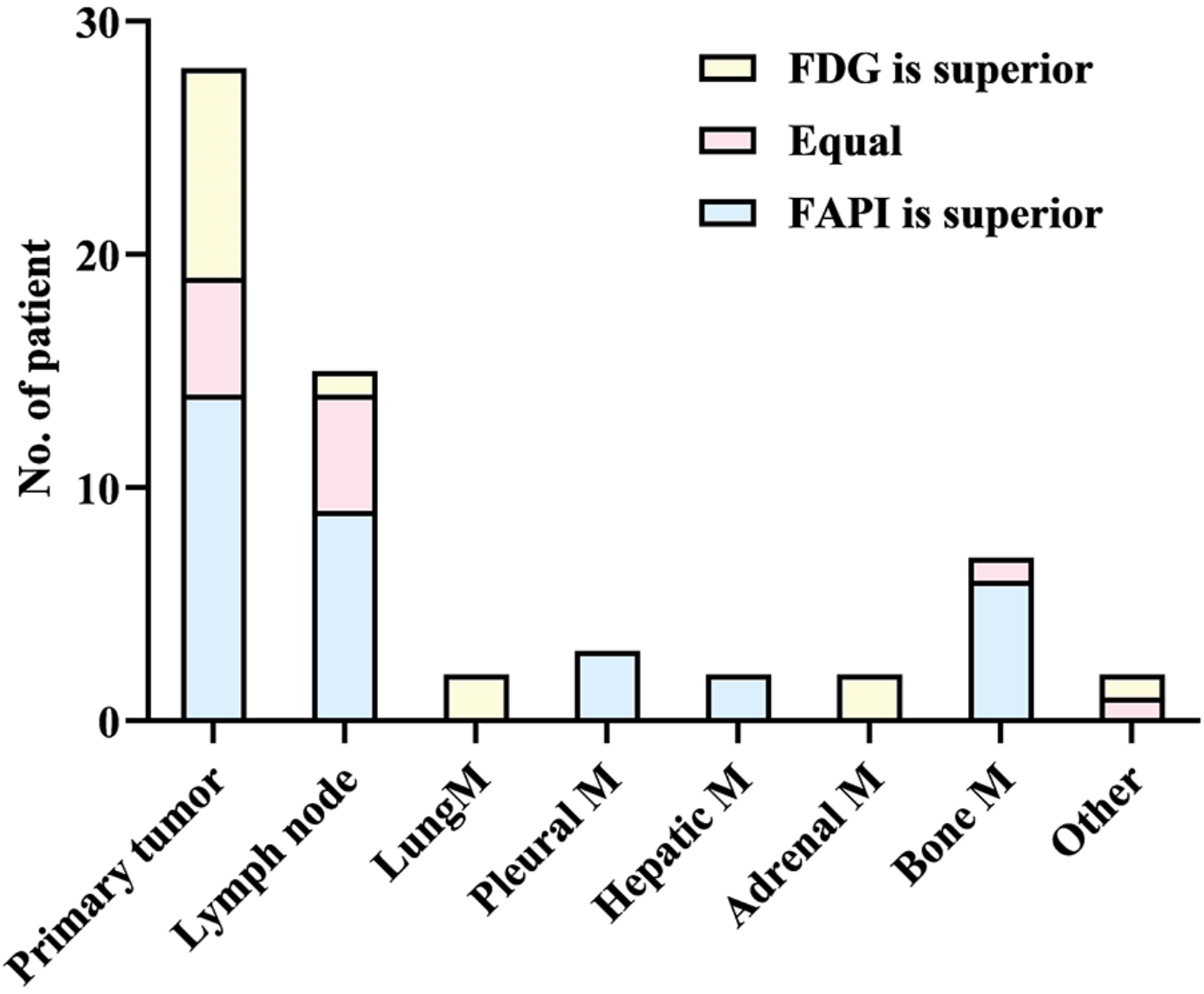

Figure 1

Visual assessment comparison for [^{18}F]FDG and [^{68}Ga]Ga-FAPI imaging approaches PET/CT; M = metastases.

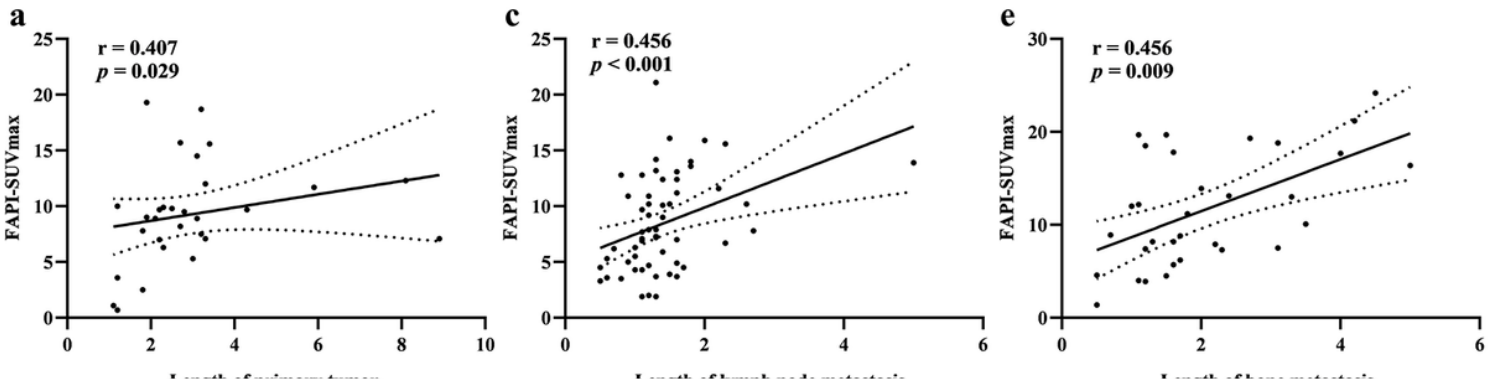

Figure 2

Spearman rank correlation analysis of the relationship between SUVmax value and lesion length for primary tumors (a. FAPI-SUVmax; b. FDG-SUVmax), lymph node metastases (c. FAPI-SUVmax; d. FDG-SUVmax), and bone metastases (e. FAPI-SUVmax; f. FDG-SUVmax).

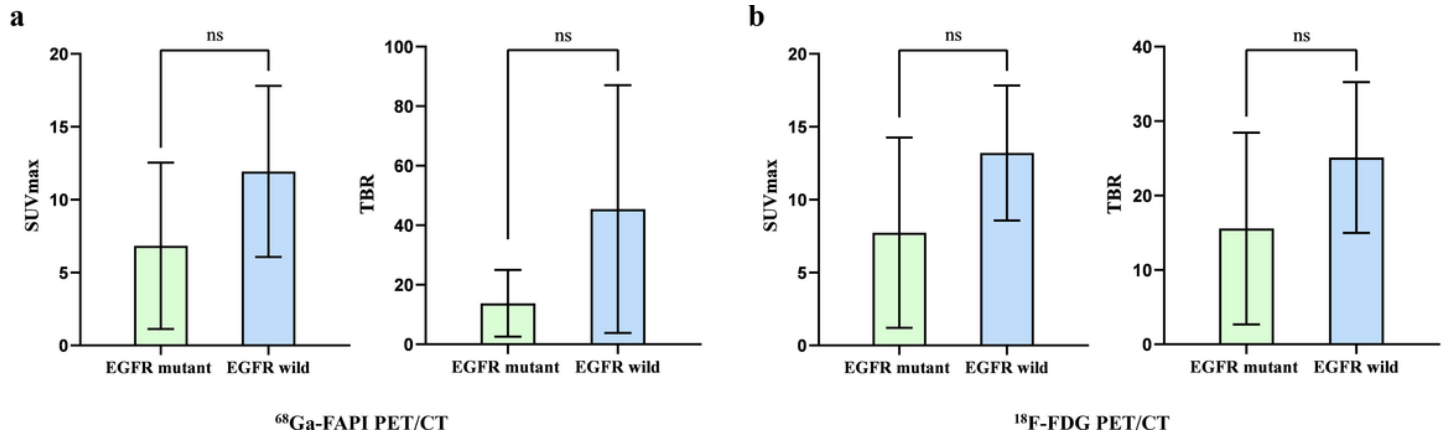

Figure 3

Metabolic parameters (SUVmax, TBR) in EGFR mutant and wild-type lung adenocarcinoma. ns = not significant.

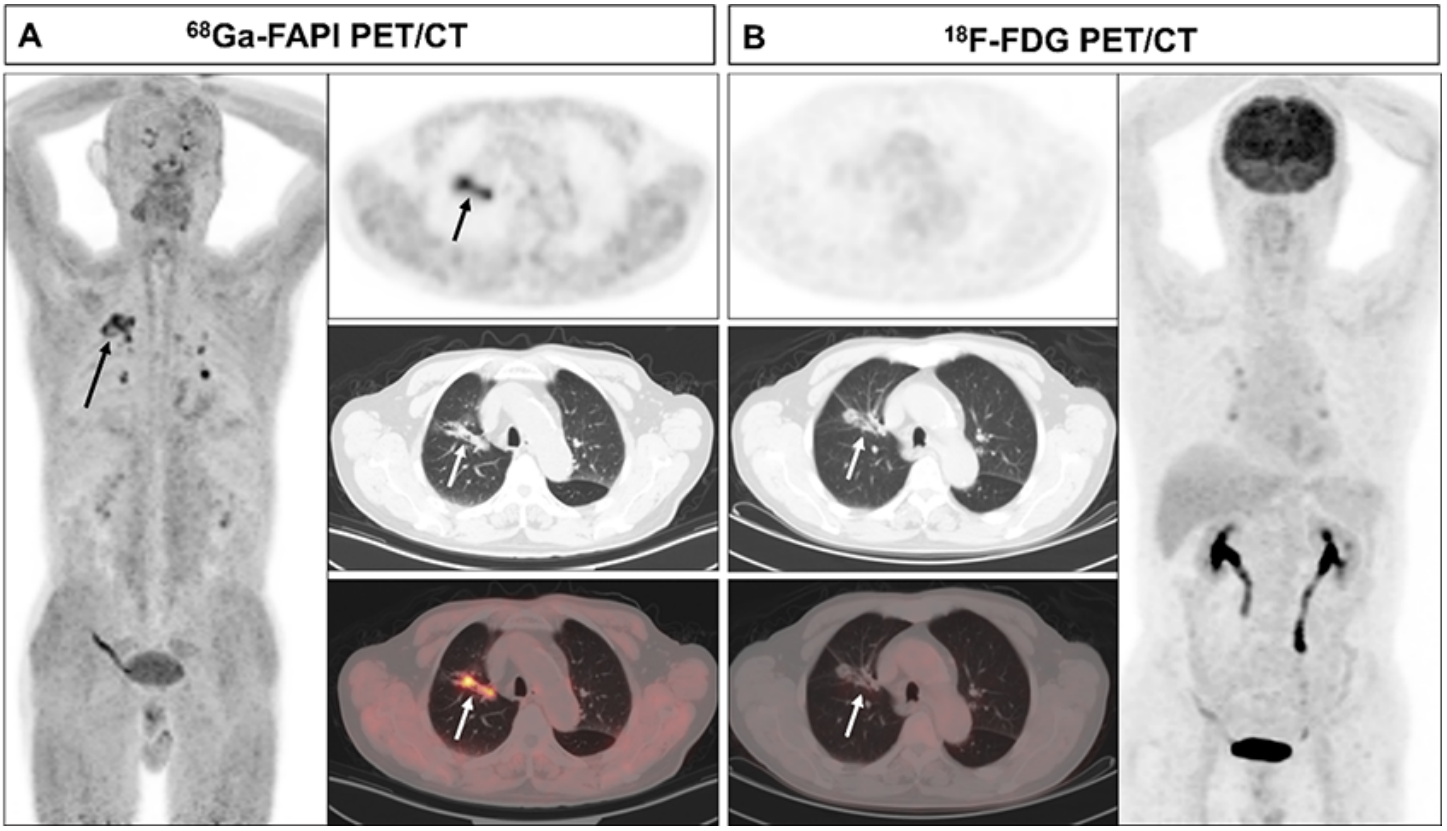

Figure 4

A 70-year-old male (patient 9) diagnosed with adenocarcinoma. [^{68}Ga]Ga-FAPI PET/CT (A) revealed an adenocarcinoma lesion with increased FAPI uptake (solid arrows, SUVmax=6.3), yet [^{18}F]FDG PET/CT imaging did not reveal any significant uptake associated with this lesion (B, solid arrows).

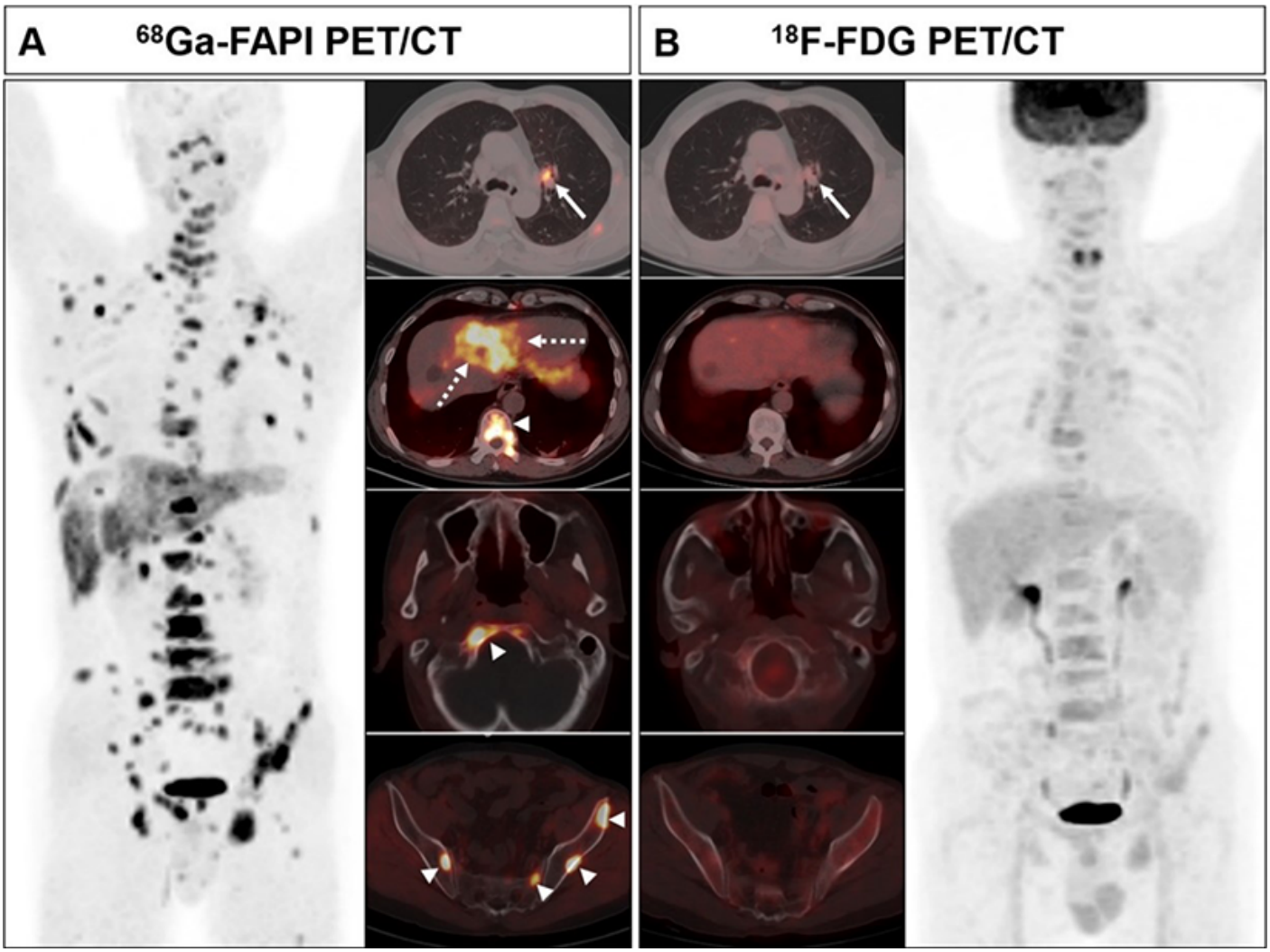

Figure 5

A 63-year-old male (patient 18) diagnosed with adenocarcinoma. [^{68}Ga]Ga-FAPI PET/CT (A) revealed intense FAPI uptake in the primary tumor (solid arrows, SUVmax = 10.0), liver metastases (dashed arrows, SUVmax = 7.6), and bone metastases (arrows, SUVmax = 8.3 - 8.5), whereas limited-to-no radiotracer uptake was detected in the primary tumor (solid arrow, SUVmax = 3.6), liver metastases, or bone metastases upon [^{18}F]FDG PET/CT imaging (B).

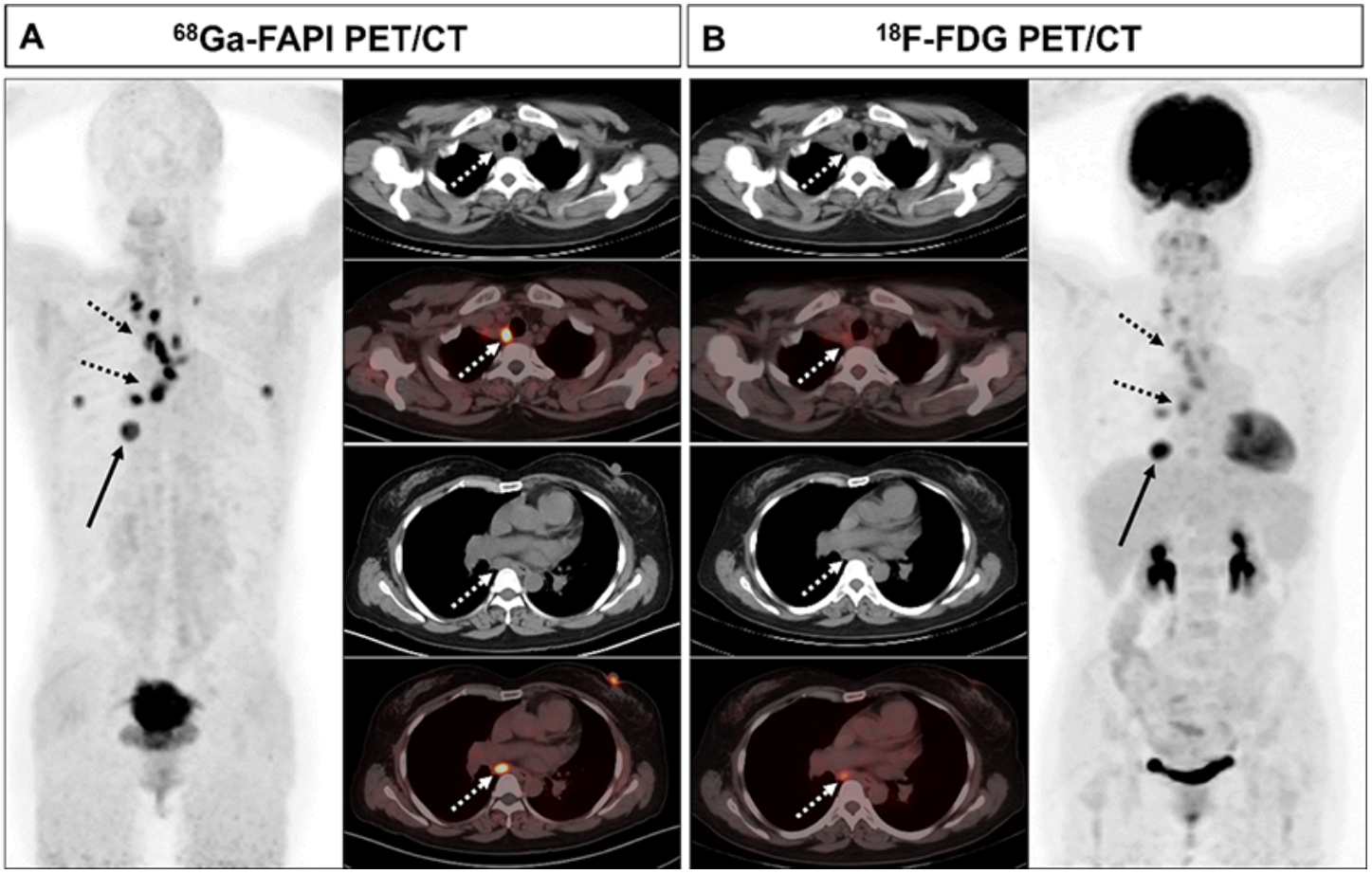

Figure 6

A 46-year-old female (patient 15) diagnosed with adenocarcinoma. [^{68}Ga]Ga-FAPI PET/CT (A) demonstrated enhanced tracer uptake in the primary adenocarcinoma lesion (solid arrow, SUVmax = 7.5), as well as intense FAPI uptake by multiple lymph nodes (dashed arrows, SUVmax= 4.0 - 11.2). [^{18}F]FDG PET/CT (B) similarly revealed high levels of radiotracer uptake by the primary adenocarcinoma lesion (solid arrow, SUVmax = 10.9), whereas only low-to-moderate FDG uptake was evident for the multiple lymph node lesions (dashed arrows, SUVmax = 2.1 - 4.8). The identified lymph node lesions were considered to be likely metastatic, as confirmed upon subsequent follow-up.

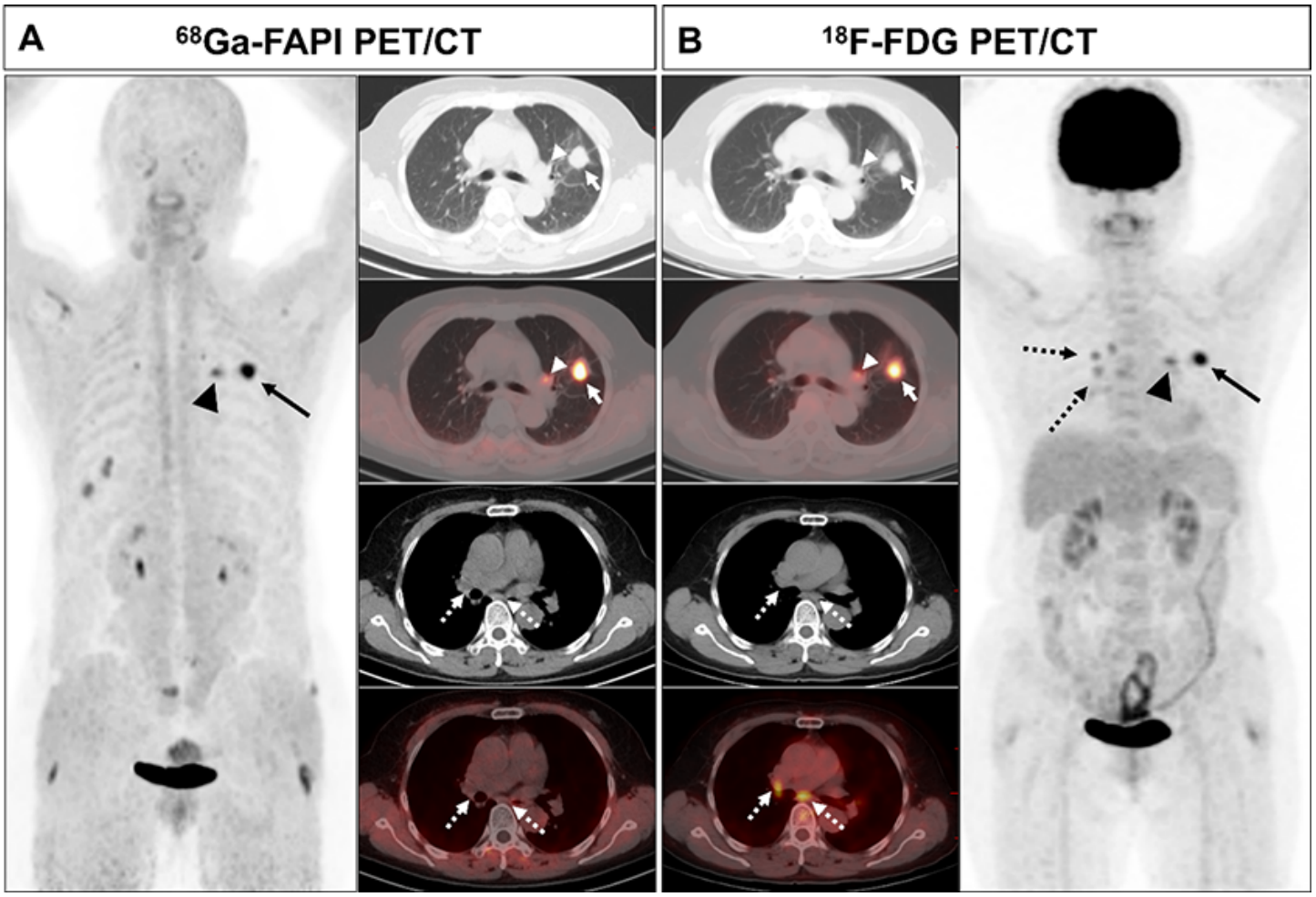

Figure 7

A 61-year-old female (patient 23) diagnosed with adenocarcinoma. [^{68}Ga]Ga-FAPI PET/CT (A) revealed intense FAPI uptake in the primary tumor (solid arrows, SUVmax = 9.7) along with moderately increased uptake in the left pulmonary hilar lymph node (arrows, SUVmax = 5.0), whereas there was no evidence of uptake in the subcarinal and right pulmonary hilar lymph nodes (dashed arrows). [^{18}F]FDG PET/CT imaging divulged intense uptake of FDG in the primary tumor (solid arrows, SUVmax = 9.0) with moderate uptake in the left pulmonary hilar (arrows, SUVmax = 4.5), subcarinal, and right pulmonary hilar (dashed arrows, SUVmax = 3.5) lymph nodes. Following mediastinal lymph node dissection, pathological biopsy verified the existence of a metastatic left pulmonary hilar lymph node, whereas no metastases were evident in the subcarinal or right pulmonary hilar lymph nodes.

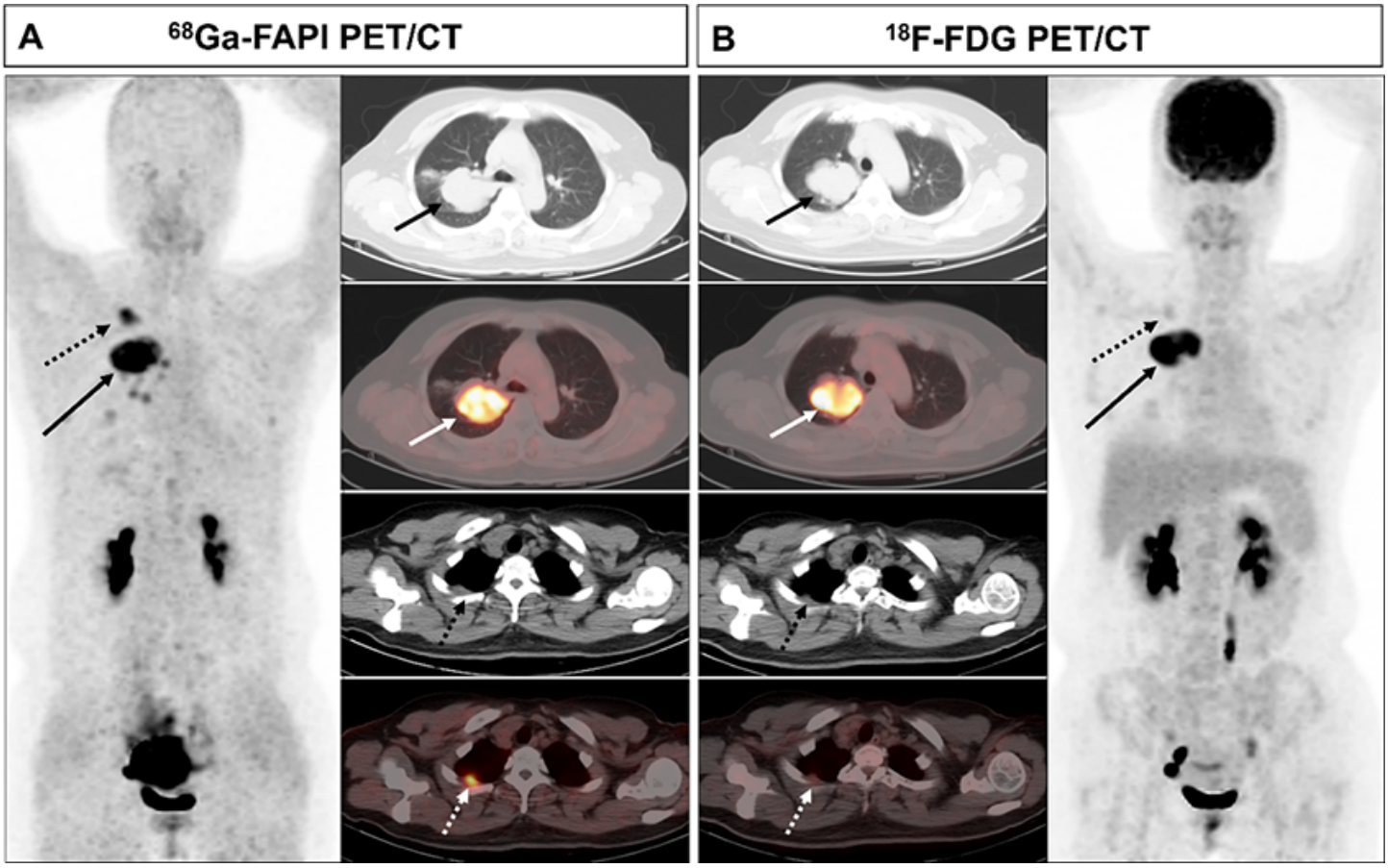

Figure 8

A 44-year-old female (patient 1) diagnosed with adenocarcinoma. [^{68}Ga]Ga-FAPI PET/CT (A) revealed intense FAPI uptake by the primary adenocarcinoma lesion (solid arrows, SUVmax = 11.7), with evidence of pleural thickening and a corresponding increase in tracer uptake (dashed arrows, SUVmax = 7.0). [^{18}F]FDG PET/CT (B) similarly revealed a high degree of FDG uptake by the primary adenocarcinoma lesion (solid arrows, SUVmax = 12.4), whereas the pleural lesion exhibited only mild radiotracer uptake (dashed arrow, SUVmax = 2.2). The pleural lesion was deemed likely to be metastatic, as confirmed upon subsequent follow-up.